Nano-electrochemistry & Nano-photochemistry
https://www.sciltp.com/journals/nenp

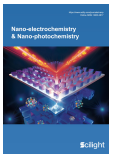

Article

Point-of-Care-Testing Method for the Detection of Antithrombotic Active Ingredients in Leech by Personal Glucose Monitor

Ruoyu Ba, Xiangyu Sun, Fen Wan, Li Zhang * and Fangfang Cheng *

Jiangsu Key Laboratory for High Technology Research of TCM Formulae, National and Local Collaborative Engineering Center of Chinese Medicinal Resources Industrialization and Formulae Innovative Medicine, Jiangsu Collaborative Innovation Center of Chinese Medicinal Resources Industrialization, Nanjing University of Chinese Medicine, Nanjing 210023, China
* Correspondence: zhangli@njucm.edu.cn (L.Z.); ffcheng@njucm.edu.cn (F.F.C.)

How To Cite: Ba, R.; Sun, X.; Wan, F.; et al. Point-of-Care-Testing Method for the Detection of Antithrombotic Active Ingredients in Leech by Personal Glucose Monitor. *Nano-electrochemistry & Nano-photochemistry* **2026**, *2*(3), 15. https://doi.org/10.53941/nenp.2026.100015

Received: 11 April 2026
Revised: 8 June 2026
Accepted: 15 June 2026
Published: 7 July 2026

Abstract: Leech is a commonly traditional Chinese medicine with antithrombotic effects. The activity of antithrombotic active ingredients in leech is an important parameter of the quality. Herein, a novel point-of-care-testing method based on antithrombin activity for detecting antithrombotic active ingredients was developed via personal glucose monitor. Fe_3O_4-PEI was synthesized via chemical coprecipitation, followed by the sequential conjugation of thrombin, thrombin aptamer, streptavidin, and invertase. Invertase catalyzed sucrose into glucose, which can be quantitatively detected using a personal glucose meter. Hirudin discovered in leeches, is the most effective thrombin inhibitor in the clinical treatment of thrombotic diseases and was used as a model drug in this work. In the presence of hirudin, it inhibited the activity of thrombin, resulting in a signal reduction in glucose. This point-of-care-testing method for hirudin activity detection exhibited a good linear range from 0.05~0.5 U mL^{-1} with a detection limit of 0.048 U mL^{-1}, providing a simple and sensitive method for the activity evaluation of antithrombotic ingredients of Chinese medicine.

Keywords: leech; Hirudin; Fe_3O_4; Point-of-Care-Testing; PGM

1. Introduction

Thrombotic diseases are pathological processes in which formed elements in the blood form clots within blood vessels, leading to partial or complete vascular obstruction and subsequent impairment of blood supply or venous return in the affected areas [1]. Leech is a common traditional Chinese medicine containing various antithrombotic ingredients. Hirudin as a well-known anticoagulant ingredient found in the saliva of leeches is widely used as an antithrombotic agent by anticoagulation effect [2]. Compared with other antithrombin drugs, it offers several advantages, including direct and irreversible inhibition of thrombin, predictable anticoagulant effects, no interference from natural anticoagulants in the body, low risk of platelet activation, stable action, and so on [3]. It consists of a single peptide chain containing 65 amino acids with a molecular weight of approximately 7 kDa [4,5]. As a potent and specific thrombin inhibitor, its dissociation constant for thrombin inhibition is as low as 20 fM [6], which directly binds to both the catalytic site and the anion-binding exosite of thrombin in a 1:1 molar ratio, thereby inhibiting thrombin activity and reducing fibrin formation [7]. To date, numerous methods have been developed for detecting hirudin activity. The most common approaches include bioactivity assays, immunoassays, and chemical analysis methods [8]. The sensitivity and the accuracy of these methods have reached a high level. However, they need complicated operation, expensive instrumentations and expert technical skills that are not applicable to on-site quality evaluation of leeches. Therefore, a simple detection method for hirudin

activity with high sensitivity, strong specificity, great simplification, and low cost is essential for practical application in the assessment of leech quality.

Point-of-care-testing (POCT), also known as "bedside testing" or "near-patient testing", offers the advantages of rapid results, simple instrument operation, wide application range, and suitability for diverse populations [9,10]. POCT methods are widely used in fields such as biomarker detection and food management [11,12]. Currently, the most widely used and well-established POCT product is the personal glucose monitor (PGM) [13]. PGM offers high sensitivity and accuracy for glucose concentration detection, along with simple operation and low cost, providing great convenience for diabetic patients to monitor their personal blood glucose changes. In essence, PGM is an enzyme-based amperometric electrochemical biosensor. When glucose oxidase reacts with glucose in the blood, electron transfer occurs and a microcurrent generates to determine the glucose concentration [14]. Leveraging the advantages of simple operation and immediate results, PGM for the detection of various biomarkers and toxic substances were continuously developed. However, direct integration of PGM for the non-glucose analyte detection still faces the shortcomings of unsatisfactory sensitivity and chemical modification or biomolecule immobilization that induced bioactivity loss of recognition antibodies.

To address the low sensitivity of PGM detection for target analytes, nanomaterials have been applied, which possess excellent properties such as a high surface area, outstanding biocompatibility, strong electrical conductivity, high loading capacity for receptor molecules, and catalytic capability [15]. Superparamagnetic iron oxide nanoparticles (SPIONs) refer to nanoparticles with a single magnetic domain and a particle size of less than 20 nm that can generate a substantial magnetic moment in the same direction under an external magnetic field and rapidly demagnetize with no hysteresis upon removal of the magnetic field [16]. SPIONs not only exhibit excellent magnetic properties, but also possess favorable physical stability and biocompatibility [17]. These unique characteristics enable their widespread application in analytical and biomedical fields, including magnetic resonance imaging [18], biocatalysis [19], magnetic hyperthermia [20], magnetic targeted delivery [21], and magnetic separation [22]. Furthermore, the surface of SPIONs can be flexibly modified with specific functional groups to meet diverse requirements.

In this study, magnetic ferroferric oxide nanomaterials (Fe_3O_4) have been modified with a signal transduction system consisting of thrombin, thrombin-targeted aptamer, streptavidin and biotin-modified invertase for the specific and sensitive detection of hirudin via PGM. Hirudin exhibited high affinity to the thrombin immobilized on the surface of Fe_3O_4 and thrombin-targeted aptamer was released, leading to the lower loading content of invertase and the corresponding reduction of glucose detected by PGM. An excellent dynamic range and novel performance for hirudin activity analysis were achieved and this proposed method was further applied in antithrombotic active ingredients of the leech extract, providing a significant protocol for routine screening and quality control of antithrombotic drug.

2. Materials and Methods

2.1. Chemicals and Reagents

$FeSO_4 \cdot 7H_2O$ was obtained from Nanjing Chemical Reagent Co., Ltd. (Nanjing, China). $FeCl_3 \cdot 6H_2O$ and polyethyleneimine (PEI) were obtained from Aladdin Reagent Co., Ltd. (Shanghai, China). Ammonium chloride (NH_4Cl), glutaraldehyde (GA), and HCl were obtained from Sinopharm Chemical Reagent Co., Ltd. (Shanghai, China). Thrombin (TB), invertase, bovine serum albumin (BSA), papain, and trypsin were obtained from Shanghai Yuanye Bio-Technology Co., Ltd. (Shanghai, China). Sucrose and hirudin were obtained from Shanghai Macklin Biochemical Co. Ltd. (Shanghai, China). Sulfo-NHS-LC-biotin sodium was obtained from Shanghai Hongye Biotechnology Co., Ltd. (Shanghai, China). Biotinylated thrombin binding aptamer (TBA, 5′-Biotin-TTTTTGGTTGGTGTGGTTGG-3′) was obtained from Sangon Biotech (Shanghai) Co., Ltd. (Shanghai, China). Streptavidin (SA) was obtained from Beijing Solarbio Science & Technology Co., Ltd. (Beijing, China). Tris was obtained from NeoFroxx GmbH. (Germany). Phosphate buffer containing KCl (PBS, 0.01 M) solutions with pH values 7.4 was Wuhan Procell Life Science & Technology Co., Ltd. (Wuhan, China). All chemicals were of analytical grade and used without further purification. Ultrapure deionized water (resistivity: 18.2 MΩ·cm) from a UPT-II-10T water purification system was used throughout the experiments.

2.2. Instrumental

Transmission electron microscopy (TEM) images were obtained on an FEI Tecnai G2 microscope operating at 120 kV. Fourier transform infrared spectroscopy (FTIR) was measured on a Thermo Scientific Nicolet iS5 (Thermo Fisher Scientific Inc., Waltham, MA, USA). Zeta potentials were measured on a Zetasizer Pro (Malvern

Instruments Ltd., Malvern, UK). Personal glucose meter and corresponding test paper were supplied by Yuwell (Zhenjiang, Jiangsu, China).

2.3. Synthesis of Fe_3O_4-PEI

Firstly, Fe_3O_4-PEI NPs were prepared via a chemical co-precipitation method with slight changes [23]. Briefly, $FeSO_4 \cdot 7H_2O$ (0.05 mol) and $FeCl_3 \cdot 6H_2O$ (0.075 mol) were solved with 50 mL of deionized water in a triple-neck round-bottom flask. The triple-neck flask was placed in a 30 °C water bath under the protection of nitrogen. 10 mL of ammonia water was added at 800 rpm, and stirred for 30 min. 0.5 g PEI with a molecular weight of 1200 was added under a stirring speed of 1000 rpm at the temperature of 86 °C for 2 h. The synthesized Fe_3O_4-PEI was magnetically separated, washed three times with deionized water, and stored in deionized water at 4 °C for later use.

2.4. Synthesis of Fe_3O_4-PEI/TB

0.6 mL Fe_3O_4-PEI (2 mg mL^{-1}), 0.1 mL GA (25%), and 1.3 mL PBS (pH = 7.4, 0.01 M) were mixed in a 2 mL EP tube and incubated at room temperature under vortexing for 1 h to allow the GA to couple with the Fe_3O_4-PEI (Fe_3O_4-PEI/GA). The obtained Fe_3O_4-PEI/GA was separated by magnetic decantation, and washed three times with PBS buffer to remove excess GA. Fe_3O_4-PEI/GA was dispersed in 1 mL PBS, and different concentrations of thrombin (2.5, 5.0, 7.5, 10.0 U) were added. After 1 h, Fe_3O_4-PEI/TB was magnetically separated, washed three times with Tris-HCl buffer (pH = 7.4, 0.02 M) and dispersed in 1 mL of Tris-HCl buffer solution.

2.5. Synthesis of Fe_3O_4-PEI/TB/TBA

1 mL Fe_3O_4-PEI/TB was thoroughly mixed with different volumes (2.5 μL, 5 μL, 7.5 μL, 10 μL) of TBA (2 OD mL^{-1}) by vortexing, and incubated at room temperature for 1 h. Then Fe_3O_4-PEI/TB/TBA was magnetically separated, washed three times with Tris-HCl buffer, and dispersed in 1 mL Tris-HCl buffer solution.

2.6. Synthesis of Fe_3O_4-PEI/TB/TBA/SA

The above-mentioned Fe_3O_4-PEI/TB/TBA was mixed with different volumes (2.5, 5.0, 7.5, 10.0 μL) of SA (1 mg mL^{-1}), and incubated at room temperature for 1 h to obtain Fe_3O_4-PEI/TB/TBA/SA, which was separated by magnetic decantation, washed three times with Tris-HCl buffer, and dispersed in 1 mL Tris-HCl buffer solution.

2.7. Synthesis of Fe_3O_4-PEI/TB/TBA/SA/Bi-Iv

The steps for preparation of biotinylated-invertase (Bi-Iv) were similar to those previously reported methods with minor modifications [24]. 500 μL invertase (5 mg mL^{-1}) and 40 μL sulfur-NHS-LC-biotin (10 mM) were mixed in a 10 kDa ultrafiltration centrifuge tube and incubated for 2 h at room temperature. Afterwards, the solution was centrifuged at 9600 rpm for 8 min twice and washed with 500 μL water for 8 times. Finally, the sediments were redispersed in 750 μL water and stored at 4 °C for subsequent research.

Fe_3O_4-PEI/TB/TBA/SA solution was mixed with different volume of the prepared Bi-Iv (2.5, 5.0, 7.5, 10.0 μL) by vortexing, and incubated at room temperature for 1 h to obtain Fe_3O_4-PEI/TB/TBA/SA/Bi-Iv, which was separated by magnetic decantation, washed three times with Tris-HCl buffer and dispersed in 1 mL Tris-HCl buffer solution.

2.8. Synthesis of Fe_3O_4-PEI/TB/TBA/SA/Bi-Iv/BSA

The synthesized Fe_3O_4-PEI/TB/TBA/SA/Bi-Iv solution was mixed with BSA to remove nonspecific adsorptive molecules, and incubated at room temperature for 1 h. Fe_3O_4-PEI/TB/TBA/SA/Bi-Iv/BSA was separated by magnetic decantation, washed three times with Tris-HCl buffer, and dispersed in 1 mL Tris-HCl buffer solution for further use.

2.9. Hirudin Activity Determination

Different concentrations of hirudin (0.05, 0.1, 0.2, 0.3, 0.4, 0.5 U mL^{-1}) were added to the Fe_3O_4-PEI/TB/TBA/SA/Bi-Iv/BSA solution, and incubated at room temperature with shaking. After 1 h, the precipitation was separated by magnetic decantation, washed three times with Tris-HCl buffer solution, and then dissolved in the solution containing 1.3 mL Tris-HCl solution and 0.2 mL sucrose (0.5 mol L^{-1}) solution. After incubation in a 55 °C water bath for 18 min, the supernatant was measured using a Yuwell 660 personal glucose meter.

2.10. Detection of Hirudin in Leech Extract

The lyophilized leech powder (46.55 mg) was weighed and dissolved in 2 mL ultrapure water. The leech extract solution (10 μL) was added to react with 1 mL Fe_3O_4-PEI/TB/TBA/SA/Bi-Iv/BSA for 1 h. The precipitation was separated by magnetic decantation, washed three times with Tris-HCl solution, and then dissolved in the solution containing 1.3 mL Tris-HCl buffer solution and 0.2 mL sucrose solution. After incubation in a 55 °C water bath for 18 min, the supernatant was measured by a Yuwell 660 personal glucose meter.

3. Results and Discussion

3.1. Principle of the Proposed PGM Strategy for Hirudin Detection

The novelty of the research focuses on the adoption of PGM for simple detection of hirudin in leech extract by taking glucose produced by sucrase catalysis as a signal reporter. How to effectively integrate the PGM with hirudin recognition event is the critical step of the hirudin detection strategy. The mechanism of PGM-based platform for hirudin activity detection was detailly depicted in Scheme 1. Fe_3O_4-PEI and thrombin were conjugated using GA as a cross-linker. The biotinylated TBA was conjugated to the TB immobilized on the Fe_3O_4-PEI. Then SA was conjugated to the biotinylated TBA via the specific recognition between SA and biotin. Subsequently, Bi-Iv was conjugated to SA, which played a critical role in generating glucose, thereby contributing to a cascade-enhanced signal amplification effect. Finally, the remaining sites on Fe_3O_4-PEI were blocked with BSA to prevent non-specific interference. The dissociation constant (K_d) of hirudin for TB is 20 fM [6], whereas that of the biotinylated TBA is 100 nM [25]. The binding affinity of hirudin to TB is significantly higher than that of the biotinylated TBA. The addition of hirudin caused the dissociation of the biotinylated TBA from TB. This dissociation led to a reduction in the amount of SA and Bi-Iv, ultimately affecting the concentration of the generated glucose. Therefore, hirudin detection can be achieved by the relationship between the hirudin activity and glucose concentration measured by PGM.

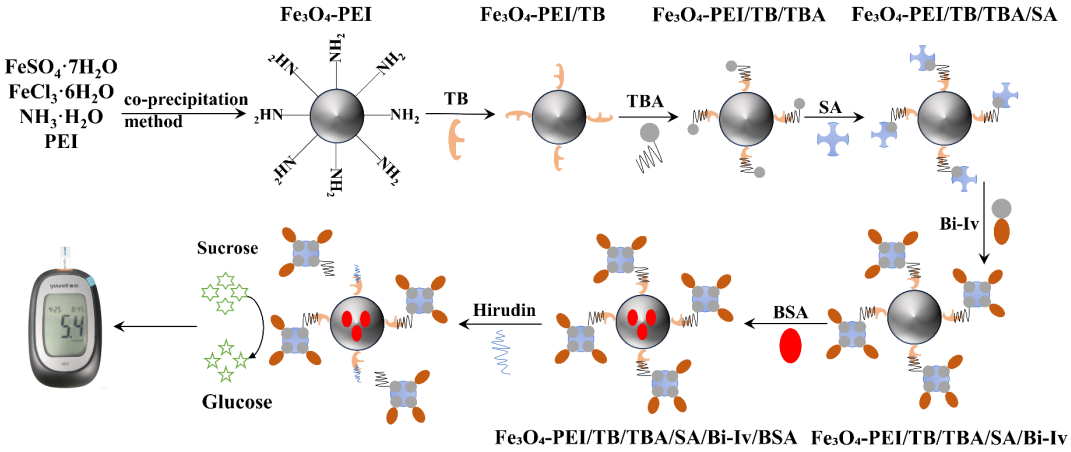

Scheme 1. Schematic diagram of the mechanism for the hirudin detection based on PGM.

3.2. Characterization of Fe_3O_4-PEI, Fe_3O_4-PEI/TB, Fe_3O_4-PEI/TB/TBA, Fe_3O_4-PEI/TB/TBA/SA, Fe_3O_4-PEI/TB/TBA/SA/Bi-Iv, Fe_3O_4-PEI/TB/TBA/SA/Bi-Iv/BSA

The morphology of Fe_3O_4-PEI was characterized by TEM, and the results showed that Fe_3O_4-PEI presented a regular spherical shape (Figure 1A). The average particle size was 11.63 ± 2.93 nm (Figure 1B). As shown in Figure 1C, Fe_3O_4-PEI exhibited a distinct absorption peak at 3411.4 cm^{-1}, which may be attributed to the stretching vibration of -N-H- bonds. The absorption peak at 2956 cm^{-1} was likely due to the symmetric stretching of -C-H- bonds. A strong absorption peak at 533.1 cm^{-1} was observed, which can be ascribed to the Fe-O bond. These results indicated that PEI was successfully modified on the surface of Fe_3O_4. Compared with Fe_3O_4-PEI, the absorption peak at 2986 cm^{-1} for Fe_3O_4-PEI/TB, Fe_3O_4-PEI/TB/TBA, Fe_3O_4-PEI/TB/TBA/SA, Fe_3O_4-PEI/TB/TBA/SA/Bi-Iv, and Fe_3O_4-PEI/TB/TBA/SA/Bi-Iv/BSA was significantly enhanced. These results suggest the successful modification of TB, TBA, SA, Bi-Iv, and BSA, leading to an increase in -C-H- absorption. Meanwhile, the absorption peak at 1630 cm^{-1} was also notably enhanced. This may be due to the superimposed absorption of carboxyl groups from TB, TBA, SA, Bi-Iv, and BSA, further confirming the successful modification of these components. In addition, the zeta potentials of Fe_3O_4-PEI, Fe_3O_4-PEI/TB, Fe_3O_4-PEI/TB/TBA, Fe_3O_4-

PEI/TB/TBA/SA, Fe_3O_4-PEI/TB/TBA/SA/Bi-Iv were measured (Figure 1D). Fe_3O_4-PEI exhibited a positive potential due to the abundant amino groups of PEI. After modification with TB and TBA, the potential gradually decreased compared to Fe_3O_4-PEI, which may be attributed to the negative charge of TB and TBA in pH 7.4 solution, leading to a decrease in zeta potential, indicating successful modification of TB and TBA. After SA modification, the potential increased compared to Fe_3O_4-PEI-TB-TBA due to the binding of SA to biotin-TBA, where the relatively large size of SA altered the conformation of TBA, leading to an increase in zeta potential and indicating successful SA modification. Following modification with Bi-Iv, the potential decreased compared to Fe_3O_4-PEI/TB/TBA/SA because Bi-Iv carried a high negative charge in pH 7.4 solution, causing a decrease in zeta potential and confirming successful Bi-Iv modification.

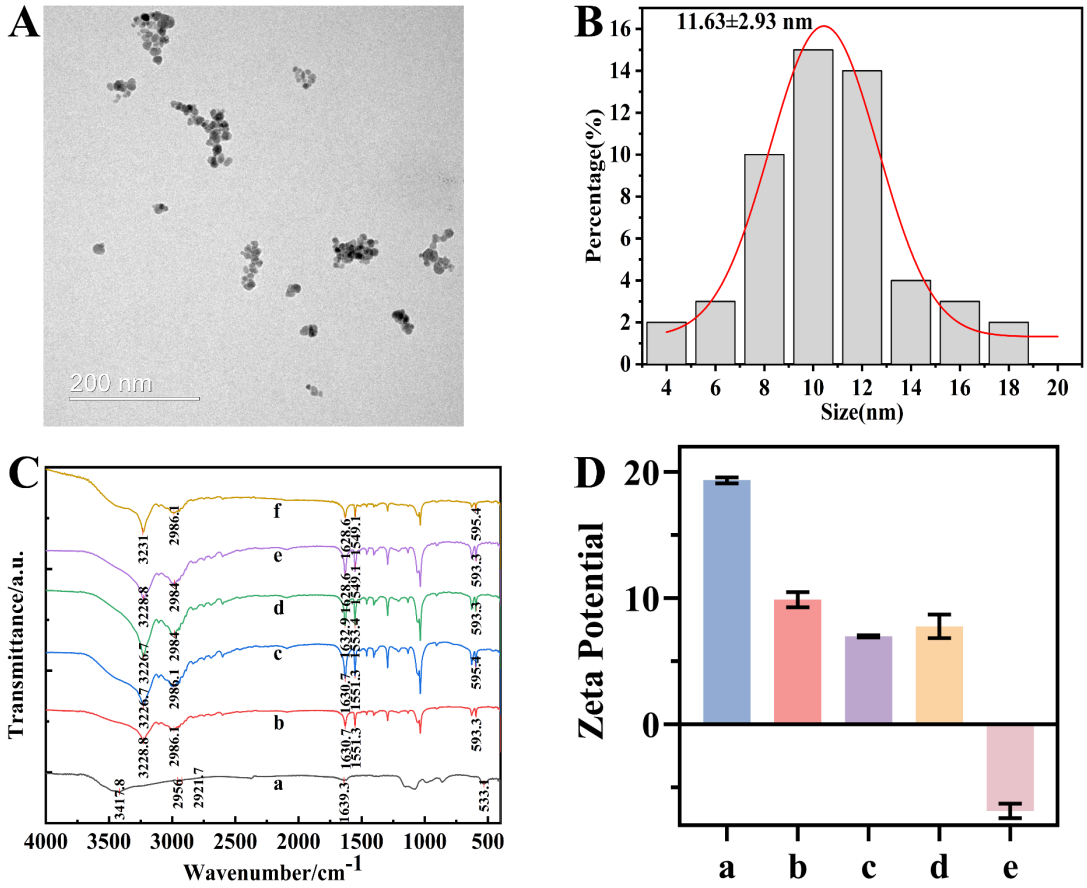

Figure 1. (**A**) TEM image of Fe_3O_4-PEI. (**B**) Particle size distribution of Fe_3O_4-PEI. (**C**) Infrared spectrum of Fe_3O_4-PEI(a), Fe_3O_4-PEI/TB(b), Fe_3O_4-PEI/TB/TBA (c), Fe_3O_4-PEI/TB/TBA/SA(d), Fe_3O_4-PEI/TB/TBA/SA/Bi-Iv(e), Fe_3O_4-PEI/TB/TBA/SA/Bi-Iv/BSA(f). (**D**) Zeta Potentials of Fe_3O_4-PEI(a), Fe_3O_4-PEI/TB(b), Fe_3O_4-PEI/TB/TBA(c), Fe_3O_4-PEI/TB/TBA/SA(d), Fe_3O_4-PEI/TB/TBA/SA/Bi-Iv(e). Error bars represented the standard deviation of three independent measurements (n = 3).

3.3. Optimization of Experimental Conditions

In order to obtain the best detection performance of the biosensor, the experimental conditions were optimized. The optimization of TB usage showed that as the amount of TB increased, the glucose concentration continuously increased (Figure 2A). Therefore, 10 U of TB was selected as the optimal dosage. The glucose concentration increased with increasing amount of TBA, reaching a maximum at 0.015 OD (Figure 2B). Thus, 0.015 OD of TBA was chosen as the optimal TBA dosage. The glucose concentration increased with increasing amount of SA, and then declined when the amount of SA was higher than 5 μg. 5 μg of SA was selected as the optimal SA dosage (Figure 2C). The glucose concentration increased continuously with increasing amount of Bi-Iv, and the optimal volume of Bi-Iv was 10 μL (Figure 2D).

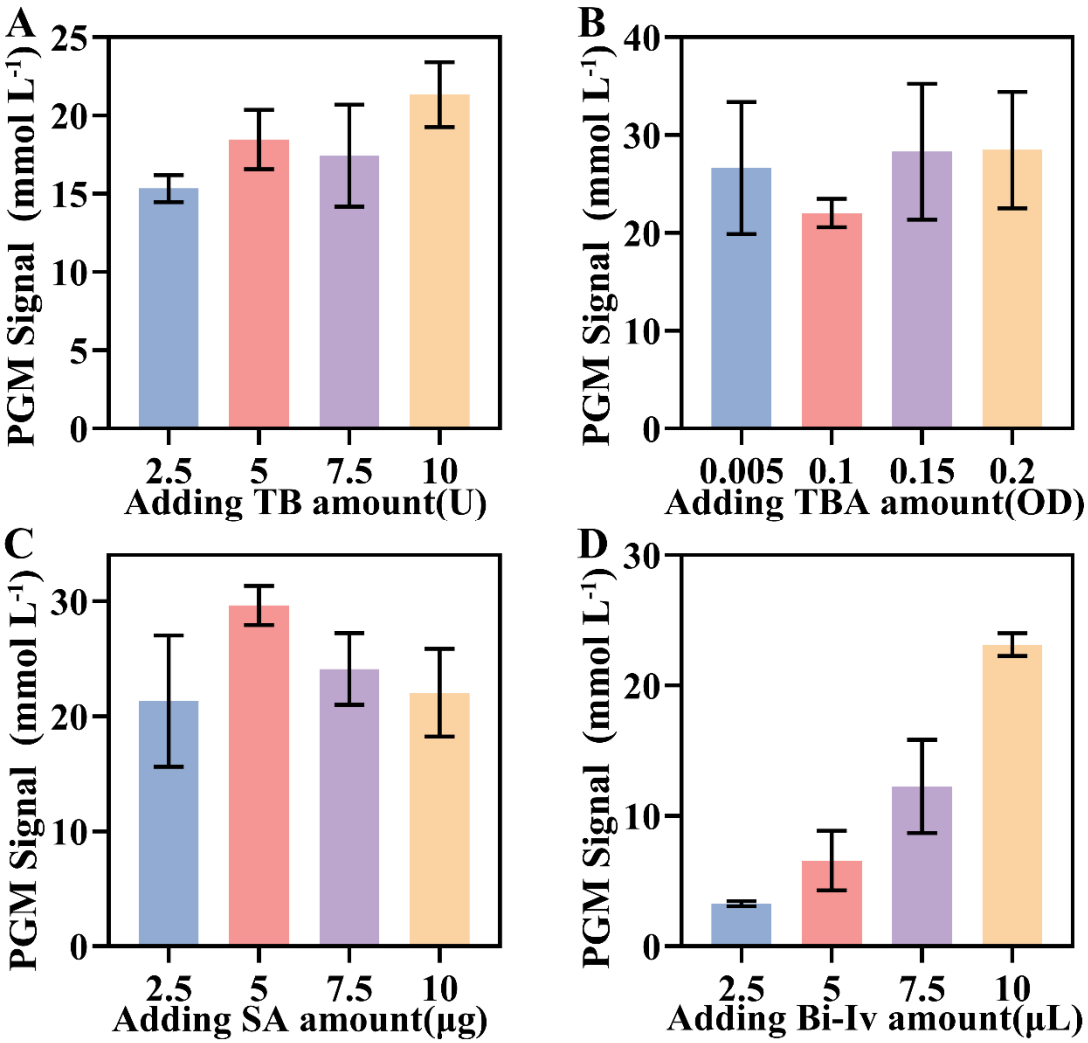

Figure 2. (**A**) Glucose concentration variation with different TB amounts. (**B**) Glucose concentration variation with different TBA amounts. (**C**) Glucose concentration variation with different SA amounts. (**D**) Glucose concentration variation with different Bi-Iv amounts. Error bars represented the standard deviation of three independent measurements (n = 3).

Additionally, the addition order of BSA was optimized. Specifically, a comparison was made between the generated glucose concentrations when BSA was added after the synthesis of Fe_3O_4-PEI/TB and Fe_3O_4-PEI-TB/TBA/SA/Bi-Iv, respectively. As shown in Figure 3A, the latter resulted in a higher glucose concentration. The probable reason was that when BSA was added after the synthesis of Fe_3O_4-PEI/TB, some of the TB was blocked and subsequently reduced the conjugation of TBA, SA, and Bi-Iv. While BSA was added after the synthesis of Fe_3O_4-PEI/TB/TBA/SA/Bi-Iv, the conjugation had a small impact on catalytic activity of Bi-Iv, so the glucose concentration did not significantly decrease. Therefore, BSA was added after the synthesis of Fe_3O_4-PEI/TB/TBA/SA/Bi-Iv. The pH value was also optimized for the hydrolysis of sucrose by invertase. The glucose concentration was measured when sucrose was hydrolyzed in Tris-HCl buffers at pH 7.4, 6.4, 5.4, and 4.4, respectively. The glucose concentration increased as the pH decreased (Figure 3B). The reason was likely that under acidic conditions, sucrose decomposed into glucose and fructose without enzymatic hydrolysis by invertase. Therefore, Tris-HCl buffer at pH 7.4 was selected to avoid the non-invertase-catalyzed sucrose hydrolysis. Moreover, the hydrolysis time for sucrose by invertase was optimized. The results indicated that the glucose concentration was highest at 18 min, and extending the time further would cause the glucose concentration to exceed the detection range of PGM (Figure 3C). Therefore, a hydrolysis time of 18 min was selected.

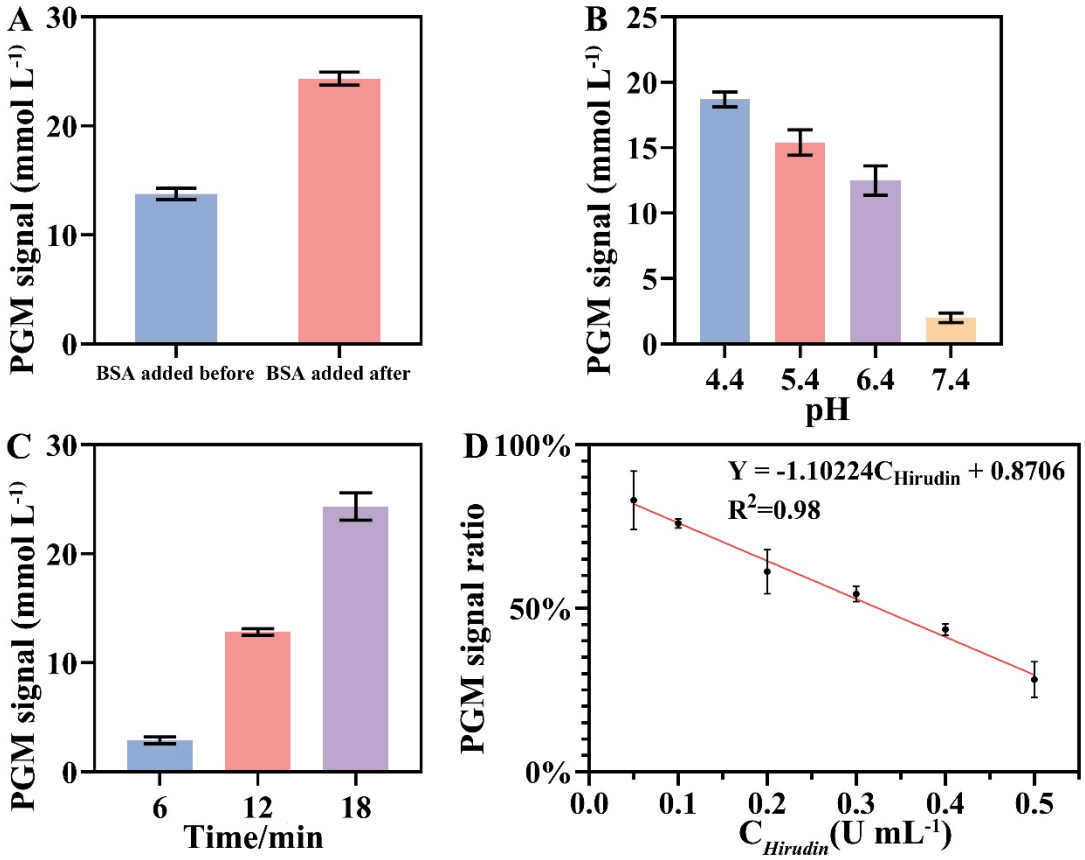

Figure 3. (**A**) Effects of the addition order of BSA on the generated glucose concentration. (**B**) Effects of pH value on the generated glucose concentration. (**C**) Effects of the incubation time on the generated glucose concentration. (**D**) Linear relationship between the PGM signal ratio (I/I_0) and the concentration of hirudin (0.05 U mL^{-1}, 0.1 U mL^{-1}, 0.2 U mL^{-1}, 0.3 U mL^{-1}, 0.4 U mL^{-1}, 0.5 U mL^{-1}). I and I_0 were the generated glucose concentrations with and without adding hirudin, respectively. Error bars represented the standard deviation of three independent measurements (n = 3).

3.4. Hirudin Activity Detection

Under the optimized conditions, hirudin activity was detected using a PGM. As shown in Figure 3D, the PGM signal ratio decreased proportionally with increasing hirudin activity. This was because the dissociation constant between hirudin and TB is smaller than that between TBA and TB. As hirudin activity increased, TBA dissociated from TB, leading to a corresponding reduction in SA and Bi-Iv, which in turn caused a decrease in glucose concentration. The PGM signal ratio exhibited a good linear relationship with the hirudin activity in the range of 0.1 U to 0.5 U mL^{-1}. The linear regression equation was $y = -1.10224C_{Hirudin} + 0.8706$, with a correlation coefficient (R^2) of 0.98. The detection limit (3.3 σ/S) was 0.048 U mL^{-1} and the quantitation limit (10 σ/S) was 0.144 U mL^{-1}. This method exhibited a narrow linear range restricted by the detection range of the portable glucose meter. Compared with other reported methods (Table 1), this work focused on hirudin activity rather than hirudin concentration, which can more accurately reflect leech quality.

Table 1. Comparison of the present method with other reported methods.

Methods	Linear range	LOD	Ref
LC-QTOF/MS	1.5–300 nM	0.5 nM	[26]
CE-LIF	14.2–144.4 nM	14.2 nM	[27]
CSA	3.12–40.0 ng mL^{-1}	3.12 ng mL^{-1}	[28]
UPLC-MS	10–2000 ng mL^{-1}	none	[29]
POCT	0.05–0.5 U mL^{-1}	0.048 U mL^{-1}	This work

3.5. Methodological Investigation

To evaluate the specificity, Fe_3O_4-PEI/TB/TBA/SA/Bi-Iv/BSA was mixed with BSA, trypsin, papain, and the mixture of hirudin and the aforementioned enzymes (Figure 4A). There were no significant differences in

glucose concentrations of BSA, trypsin, papain group relative to the blank group. The glucose concentrations of all mixture groups were similar to the hirudin group. These results indicated this method exhibited a good anti-interference performance and high specificity. In addition, the effects of the other thrombin inhibitors argatroban and bivalirudin were also investigated (Figure 4B). After the addition of argatroban and bivalirudin, no significant differences in the glucose concentration were measured compared to the blank group. The probable reason was that argatroban only bound to the other active site of TB, without affecting the specific binding between TBA and TB, thus having no impact on glucose production. Although bivalirudin shared the same binding site to TB as TBA, it failed to compete with TBA because of its larger molecular weight and greater steric hindrance. These results indicated this POCT method based on antithrombin activity for detecting antithrombotic active components demonstrated good selectivity for hirudin and was not affected by other thrombin inhibitors.

The stability and reproducibility experiments of the method were also examined. Fe_3O_4-PEI/TB/TBA/SA/Bi-Iv/BSA was used to hydrolyze sucrose at 1 h, 12 h, 24 h, and 48 h, respectively. No significant difference in the glucose concentration was measured, demonstrating its good stability (Figure 4C). The intra-day and inter-day precision presented RSD of 3.6% and 1.9%, respectively, indicating this method had an acceptable precision (Tables 2 and 3).

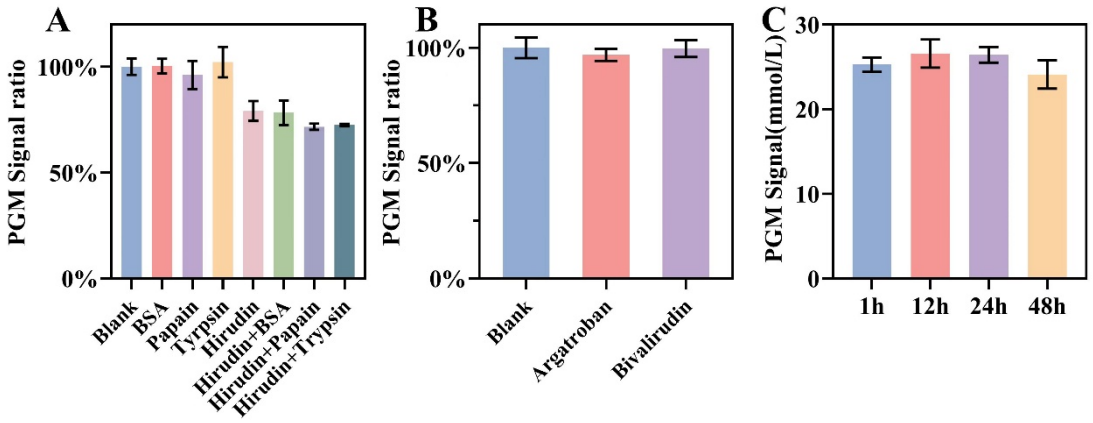

Figure 4. (**A**) Specificity experiment for POCT detection of hirudin activity. (**B**) Interference experiment for POCT detection of hirudin activity. (**C**) Stability experiment for POCT detection of hirudin activity. Error bars represented the standard deviation of three independent measurements (n = 3).

Table 2. Intra-day precision.

	Group 1	Group 2	Group 3	RSD
PGM signal (mmol L^{-1})	25.5	23.9	24.1	3.6%

Table 3. Inter-day precision.

	Day1	Day2	Day3	RSD
PGM signal (mmol L^{-1})	25.3	24.7	24.4	1.9%

3.6. Detection of Antithrombotic Active Ingredients in Leech Extract

The established method was used to detect the activity of antithrombotic active ingredients in leech samples. The PGM signal ratio of leech extract added relative to was 68.8% (Table 4). Substituting this value into the standard curve, the activity of the antithrombotic active ingredient in the crude leech extract was calculated as 0.166 U mL^{-1}, equivalent to 711.8 U g^{-1} in terms of hirudin.

Simultaneously, a recovery test was conducted. The average PGM signal ratio of the mixture of hirudin and leech extract group was 57.4%, respectively (Table 4). The recovery rate was about 103%, indicating this method was reliable.

Table 4. PGM signal ratio in recovery test.

	Group 1	Group 2	Group 3	Calculated Concentration (U mL^{-1})
10 μL Leech Extract	66.3%	69.8%	70.3%	0.166
0.1 U Hirudin + 10 μL Leech Extract	56.8%	58.1%	57.3%	0.269

4. Conclusions

In summary, a POCT method was developed for the simple, selective and sensitive detection of hirudin activity via PGM. Fe_3O_4 nanoparticles were employed as a carrier to immobilize sequentially thrombin, thrombin-targeted aptamer, and streptavidin, and invertase. Based on the higher affinity between thrombin and hirudin, thrombin-targeted aptamers were displaced from the surface of Fe_3O_4, leading to decreased loading of immobilized invertase and less production of its catalytic product, glucose. The optimal usage of TB, TBA, SA, and Bi-IV, pH value, and incubation time were 10.0 U, 0.015OD, 5 μg, 10 μL, 7.4 and 18 min, respectively. The proposed method exhibited a good linear relationship between the PGM signal ratio and the hirudin activity in the range of 0.05~0.5 U mL^{-1} with a detection limit of 0.048 U mL^{-1}, as well as an excellent specificity and selectivity. It was further used to access the hirudin-like components in the leech extract with a good recovery rate, indicating this POCT approach provides a new platform for the accurate determination of the active components in traditional Chinese medicine.

Author Contributions

R.B.: investigation, data curation, writing—original draft preparation; X.S.: investigation; F.W.: investigation; L.Z.: conceptualization, funding acquisition; F.-F.C.: supervision, conceptualization, writing—reviewing and editing, funding acquisition. All authors have read and agreed to the published version of the manuscript.

Funding

The authors are thankful to the National Natural Science Foundation of China (No. 82374039), Project funded by Jiangsu Administration of Traditional Chinese Medicine (No.MS2025008), Scientific Research Cultivation Project of First-class Discipline of Traditional Chinese Medicine in Nanjing University of Chinese Medicine (No. ZYXPY2024-003).

Data Availability Statement

All data are available in the article. Additional requests can be directed to the corresponding author.

Conflicts of Interest

The authors declare no conflict of interest.

Use of AI and AI-Assisted Technologies

No AI tools were utilized for this paper.

References

1. Wei, Y.; Yuan, X.; Zhang, X.; et al. Recent advances of organic small molecule-based fluorescent probes in bioimaging and photo-mediated therapy for thrombotic diseases. *Coord. Chem. Rev.* **2026**, *550*, 217352.
2. Yi, X.; Wu, X.; Zang, E.; et al. Construction of safer hirudin-derived peptides with enhanced anticoagulant properties based on C-terminal active residue adaptation and modification. *J. Adv. Res*. **2026**, *80*, 1083–1098.
3. Johnson, P.H. Hirudin: Clinical potential of a thrombin inhibitor. *Annu. Rev. Med*. **1994**, *45*, 165–177.
4. Chen, J.; Xie, X.; Zhang, H.; et al. Pharmacological Activities and Mechanisms of Hirudin and Its Derivatives-A Review. *Front. Pharmacol*. **2021**, *12*, 660757.
5. Markwardt, F. Hirudin as alternative anticoagulant—A historical review. *Semin. Thromb. Hemost*. **2002**, *28*, 405–414.
6. De Vincenzo, F.; Acquasaliente, L.; Pontarollo, G.; et al. Noncoded aminoacids in protein engineering: Structure–activity relationship studies of hirudin–thrombin interaction. *Biotechnol. Appl. Biochem.* **2018**, *65*, 69–80.
7. Troisi, R.; Balasco, N.; Autiero, I.; et al. Exosite binding in thrombin: A global structural/dynamic overview of complexes with aptamers and other ligands. *Int. J. Mol. Sci.* **2021**, *22*, 10803.
8. Li, B.; Ou, Y.; Wu, Y.; et al. Progress in analytical methods of hirudin. *Chin. J. Pharm. Anal*. **2010**, *30*, 755–760.
9. Bikker, R.; Meyer, K.; Domberg, P.; et al. Development and evaluation of point-of-care testing recertification with e-learning. *Scand. J. Clin. Lab. Investig.* **2020**, *80*, 133–138.
10. Haggerty, L.; Tran, D. Cholesterol Point-of-Care Testing for community pharmacies: A review of the current literature. *J. Pharm. Pract*. **2017**, *30*, 451–458.
11. Fu, D.L.; Zhang, B.; Zhang, S.; et al. An electrochemical point-of-care testing device for specific diagnosis of the albinism biomarker based on paradigm shift designs. *Biosens. Bioelectron.* **2024**, *264*, 116645.
12. Wang, Y.; Wang, M.L.; Cui, J.R.; et al. Portable devices and machine learning-assisted lateral flow assay for food safety

analysis: Developments and perspectives. *Trends Food Sci. Tech.* **2025**, *163*, 105180.
13. Yang, D.; Geng, S.; Jing, R.; et al. Recent developments in personal glucose meters as point-of-care testing devices (2020–2024). *Biosensors* **2024**, *14*, 419.
14. Huang, Q.; Chen, J.; Zhao, Y.; et al. Advancements in electrochemical glucose sensors. *Talanta* **2025**, *281*, 126897.
15. Li, L.; Wang, T.; Zhong, Y.; et al. A review of nanomaterials for biosensing applications. *J. Mater. Chem. B* **2024**, *12*, 1168–1193.
16. Girardet, T.; Bianchi, E.; Henrionnet, C.; et al. SPIONs magnetic nanoparticles for MRI applications: Microwave synthesis and physicochemical, magnetic and biological characterizations. *Mater. Today Commun*. **2023**, *36*, 106819.
17. Ramimoghadam, D.; Bagheri, S.; Abd Hamid, S.B. Stable monodisperse nanomagnetic colloidal suspensions: An overview. *Colloids Surf. B* **2015**, *133*, 388–411.
18. Zhang, Z.; Lv, M.; Hu, W.; et al. Peptide based covalent organic framework for the magnetic resonance imaging-mediated attenuation of amyloid-β fibrils. *Adv. Funct. Mater*. **2026**, e29220.
19. Wang, J.; Feng, K.; Yu, P.; et al. Iron-based nanozymes: From mechanisms to functional applications. *Chem. Eng. J*. **2026**, *539*, 177195.
20. Zhang, R.; Li, Y.; Yan, H.; et al. Breaking the trade-off in MPI-guided magnetic hyperthermia by tailoring the dynamic magnetization of magnetic nanoparticles via site-selective trace doping. *J. Am. Chem. Soc*. **2026**, *148*, 18482–18496.
21. Zhang, D.; Zhu, O.; Mou, F.; et al. Systemic-to-local nanorobot thrombolysis. *Sci. Adv*. **2026**, *12*, eaed9464.
22. Chen, Z.; Lal, K.; Wang, A.; et al. Plasmonic magnetic nanoparticle-based photothermal sensor for sensitive detection of chlorantraniliprole. *Food Chem*. **2026**, *508*, 148487.
23. Wang, T.; Hu, X.; Yang, Y.; et al. New insight into assembled Fe_3O_4@PEI@Ag structure as acceptable agent with enzymatic and photothermal properties. *Int. J. Mol. Sci.* **2022**, *23*, 10743.
24. Zhang, R.; Yan, C.; Zong, Z.; et al. Taking glucose as intermediate bridge-signal-molecule for on-site and convenient detection of ochratoxin A in rice with portable glucose meter. *Food Chem*. **2023**, *400*, 134007.
25. Bai, Y.; Li, Y.; Zhang, D.; et al. Enhancing the affinity of anti-human α-thrombin 15-mer DNA aptamer and anti-immunoglobulin E aptamer by polyT extension. *Anal. Chem*. **2017**, *89*, 9467–9473.
26. Cao, X.; Luo, Y.; Liu, X.; et al. Aptamer-thrombin loaded magnetic microspheres for bio-specific extraction and precise detection of hirudin. *Talanta* **2024**, *267*, 125244.
27. Ban, E.; Nam, H.S.; Yoo, Y.S. Competitive immunoassay for recombinant hirudin using capillary electrophoresis with laser-induced fluorescence detection. *J. Chromatogr. A* **2001**, *924*, 337–344.
28. Jiang, S.; Jiao, J.; Zhang, T.; et al. Pharmacokinetics study of recombinant hirudin in the plasma of rats using chromogenic substrate, ELISA, and radioisotope assays. *PLoS ONE* **2013**, *8*, e64336.
29. Dong, X.; Meng, Z.; Jin, J.; et al. Development, validation, and clinical pharmacokinetic application of ultra-performance liquid chromatography/tandem mass spectrometry method for simultaneously determining a novel recombinant hirudin derivative (Neorudin) and its active metabolite in human serum. *J. Chromatogr. B* **2017**, *1063*, 204–213.